J|A|C|S
ARTICLES

Published on Web 04/08/2009

Metal-Induced Folding of Diels−Alderase Ribozymes Studied by Static and Time-Resolved NMR Spectroscopy

Vijayalaxmi Manoharan,[†] Boris Fürtig,[†,§] Andres Jäschke,[‡] and Harald Schwalbe*[,†]

Center for Biomolecular Magnetic Resonance, Institute of Organic Chemistry and Chemical Biology, Johann Wolfgang Goethe-University Frankfurt, Max-von-Laue-Strasse 7, D-60438 Frankfurt/Main, Germany, and Institute of Pharmacy and Molecular Biotechnology, Heidelberg University, D-69120 Heidelberg, Germany

Received January 13, 2009; E-mail: schwalbe@nmr.uni-frankfurt.de

Abstract: The metal ion-induced folding of the Diels−Alder ribozyme into a catalytically active form with a complex RNA pseudoknot has been characterized by static and time-resolved NMR spectroscopy. The conformations of two sequences from the Diels−Alder ribozyme family, A27 WT and G27 MUT, were studied in the absence and presence of metal ions and of ligand. The single nucleotide mutant G27 MUT in the absence of metal ions displayed conformational heterogeneity which greatly influences its folding trajectory. Time-resolved NMR experiments were applied using a sample-mixing technique to rapidly add Ca^{2+} ions to induce folding in situ. The folding rates observed for the G27 MUT ribozyme differed by 3 orders of magnitude from the A27 WT folding rates determined previously by FRET experiments. A model based on the characterization of the free and metal-bound forms of the ribozymes is proposed to account for the difference in the folding rates of the two ribozymes. Evidence is provided that the reactivity is modulated due to local dynamics around the catalytic pocket for the G27 MUT ribozyme.

Introduction

The Diels−Alder reaction is one of the most important reactions in synthetic organic chemistry. It is not surprising that much effort has been directed toward developing catalysts that improve both rate and selectivity of the cycloaddition.[1−6] Among these catalysts, several classes of biological macromolecular catalysts have been developed, including catalytic antibodies,[7−9] a DNA-based hybrid catalyst,[10] two ribozymes, [11,12] and a DNA-based DNAzyme.[13] The Diels−Alder ribozyme investigated here is an in vitro selected RNA developed in the Jäschke laboratory that catalyzes the cycloaddition of anthracene dienes and maleimide dienophiles.[12] From the 16 independent RNA sequence families isolated from the initial combinatorial RNA library (2×10^{14} species, 120 randomized positions),[14] 13 contained a common small secondary structure motif consisting of an asymmetric bulge, at least three helices and a pseudoknot as overall RNA fold. A minimal 49mer RNA acts as a true catalyst by accelerating the bimolecular reaction in solution.[15] The catalysis was found to depend strongly on divalent cations such as Mg^{2+} or Mn^{2+}. The ribozyme performs the reaction with high enantioselectivity (>95% ee) and multiple turnovers (k_{cat} of 20 min^{-1}). Initial chemical substitution analysis of the RNA−substrate interactions pointed to hydrophobic and van der Waals interactions[16] between the ribozyme and the substrate while hydrogen bonding and metal ion coordination appeared to be less important in the catalysis.

Mutation and probing studies further characterized the complex structure of the ribozyme revealing the participation of the conserved asymmetric bulge region in the catalytic site.[17] It was proposed that the presence of the two reactants of the Diels−Alder reaction within the confined space of a cavity provided by the ribozyme drives the reaction.[18] Also, at high Mg^{2+} ion concentrations, the ribozyme showed no major

[†] Johann Wolfgang Goethe-University Frankfurt.
[‡] Heidelberg University.
[§] Present address: Max F. Perutz Laboratories, Department of Biochemistry, A-1030 Vienna, Austria.

(1) Ose, T.; Watanabe, K.; Mie, T.; Honma, M.; Watanabe, H.; Yao, M.; Oikawa, H.; Tanaka, I. *Nature (London)* **2003**, *422*, 185–9.
(2) Pindur, U.; Lutz, G.; Otto, C. *Chem. Rev.* **1993**, *93*, 741–761.
(3) Guimaraes, C. R. W.; Udier-Blagovic, M.; Jorgensen, W. L. *J. Am. Chem. Soc.* **2005**, *127*, 3577–3588.
(4) Watanabe, K.; Mie, T.; Ichihara, A.; Oikawa, H.; Honma, M. *J. Biol. Chem.* **2000**, *275*, 38393–38401.
(5) Katayama, K.; Kobayashi, T.; Oikawa, H.; Honma, M.; Ichihara, A. *Biochim. Biophys. Acta* **1998**, *1384*, 387–395.
(6) Auclair, K.; Sutherland, A.; Kennedy, J.; Witter, D. J.; Van den Heever, J. P.; Hutchinson, C. R.; Vederas, J. C. *J. Am. Chem. Soc.* **2000**, *122*, 11519–11520.
(7) Hilvert, D.; Hill, K. W.; Nared, K. D.; Auditor, M. T. M. *J. Am. Chem. Soc.* **1989**, *111*, 9261–9262.
(8) Braisted, A. C.; Schultz, P. G. *J. Am. Chem. Soc.* **1990**, *112*, 7430–7431.
(9) Lerner, R. A.; Benkovic, S. J.; Schultz, P. G. *Science* **1991**, *252*, 659–667.
(10) Roelfes, G.; Feringa, B. L. *Angew. Chem., Int. Ed.* **2005**, *44*, 3230–3232.
(11) Tarasow, T. M.; Tarasow, S. L.; Eaton, B. E. *Nature (London)* **1997**, *389*, 54.
(12) Seelig, B.; Jäschke, A. *Chem. Biol.* **1999**, *6*, 167–176.
(13) Chandra, M.; Silverman, S. K. *J. Am. Chem. Soc.* **2008**, *130*, 2936–2937.
(14) Jäschke, A. *Biol. Chem.* **2001**, *382*, 1321–1325.
(15) Seelig, B.; Keiper, S.; Stuhlmann, F.; Jäschke, A. *Angew. Chem., Int. Ed.* **2000**, *39*, 4576–4579.
(16) Stuhlmann, F.; Jaschke, A. *J. Am. Chem. Soc.* **2002**, *124*, 3238–3244.
(17) Keiper, S.; Bebenroth, D.; Seelig, B.; Westhof, E.; Jäschke, A. *Chem. Biol.* **2004**, *11*, 1217–1227.
(18) Kim, S. P.; Leach, A. G.; Houk, K. N. *J. Org. Chem.* **2002**, *67*, 4250–4260.

changes on substrate or product binding consistent with a preformed structure of the ribozyme.[17] The crystal structure of the ribozyme in its product bound and unbound state was determined and confirmed all the previous studies.[19]

EPR spectroscopic studies indicated different affinities and occupation for five metal(II) ion binding sites[20] and a recent study of the dynamics using single-molecule FRET spectroscopy provided insight into the structural dynamics of the wild-type ribozyme.[21] Three states, the unfolded, intermediate, and folded states, were identified and proposed to correspond to (largely) random coil, and states with secondary structure and complex native fold, respectively. The population of these states was shown to depend on the Mg^{2+} concentration and the entire RNA was shown to fluctuate permanently between these states.

In the present study, we employed NMR spectroscopy to characterize the ribozyme in the absence of Diels−Alder product and divalent ions (free form) and in the presence of product and divalent ions (complex form) by static NMR experiments, since the ribozyme does not bind the reaction product in the absence of divalent cations. We analyzed the changes in structure and dynamics upon addition of divalent ions. Furthermore, we characterized the metal-induced folding kinetics of the Diels−Alderase ribozyme by time-resolved NMR spectroscopy.

For a long time, NMR spectroscopy has been an invaluable tool to study the structure and function of nucleic acids.[22−24] Recently, time-resolved NMR experiments were developed to characterize folding transitions of biomolecules.[25−29] Bistable RNAs adopt two folds of similar stability.[30,31] We reported the kinetic characterization of the refolding between the those forms of bistable RNAs[32,33] and the folding kinetics of hypoxanthine-induced folding of a guanine-sensing riboswitch aptamer domain using chemical caging techniques.[34,35] Here, we used rapid-mixing techniques to characterize RNA-folding, a technique thus far only applied for time-resolved NMR studies of protein folding.[36] By injecting Ca^{2+} into an NMR tube containing RNA and the ligand, rapid mixing was achieved inducing Ca^{2+}-dependent folding of the RNA and monitored by 1D NMR

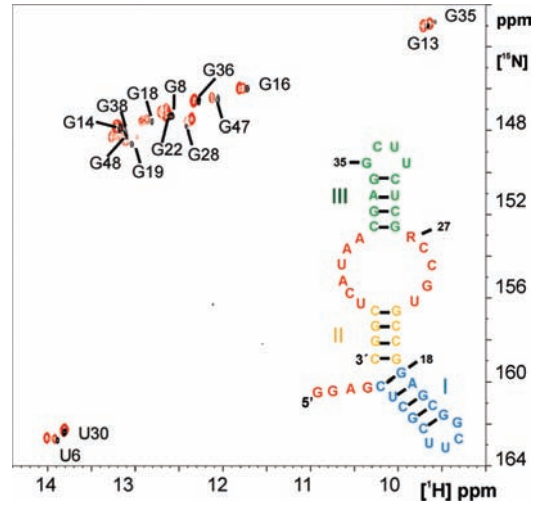

Figure 1. Overlay of $^{1}H,^{15}N$ HSQC experiment of the imino ^{1}H resonance region of the free A27 WT ribozyme in black free G27 MUT ribozyme in red. Both spectra were recorded in the absence of divalent metal ions and ligand (for experimental parameters see entries 1 and 2 in Table S2 in the Supporting Information.) The inset shows the secondary structure of the A27 WT ribozyme as predicted by mfold.[43,44] The resonances of the A27 WT ribozyme are annotated.

experiments. We substituted Ca^{2+} for Mg^{2+}, as Ca^{2+} significantly increased the stability of the complex between RNA and divalent ions and revealed favorable well-resolved NMR spectra.

For our study, we investigated two sequences of the Diels−Alderase ribozyme family: the best catalyst (A27 WT, the A27 wild-type of the 49-mer Diels–Alder ribozyme) and a single-nucleotide mutant (G27 MUT, the G27 mutant of the 49-mer Diels–Alder ribozyme) with ~70% catalytic efficiency relative to the wild-type ribozyme. The single mutation is at the junction of stem III and the asymmetrical bulge region of the ribozyme in its free form (represented by R in the secondary structure inset in Figure 1). For both forms of the ribozyme, crystal structures are available for the product-bound complex at resolutions of 3.3 Å for A27 WT and 3.0 Å for the G27 MUT. For the A27 WT, a crystal structure of the ribozyme without a bound product but in presence of Mg^{2+} is also available at a resolution of 3.5 Å.[19] Our initial time-resolved NMR experiments on the A27 WT revealed that the kinetics of ligand binding and subsequent folding is very fast and is completed within the dead time of the NMR experiment. This observation was in agreement with the FRET study that reported A27 WT folding in the order of 100 ms.[21] Therefore, for the time-resolved studies, we concentrated on the G27 MUT which showed slower folding rates. Our studies reveal that the conformation of the free forms of the wild-type and the mutant ribozyme are markedly different and that both ribozymes show significantly different folding rates.

Methods and Materials

RNA Preparation. $^{15}N,^{13}C$-labeled and unlabeled G27 MUT were prepared by in vitro transcription with T7 RNA polymerase from linearized plasmid DNA templates following literature procedures.[22] The crude runoff transcript was purified by an anion-exchange column step for removal of abortive products and unused nucleotides,[37] followed by 'ion-pair'-reversed phase

(19) Serganov, A.; Keiper, S.; Malinina, L.; Tereshko, V.; Skripkin, E.; Höbartner, C.; Polonskaia, A.; Phan, A. T.; Wombacher, R.; Micura, R.; Dauter, Z.; Jäschke, A.; Patel, D. J. *Nat. Struct. Mol. Biol.* **2005**, *12*, 218–224.
(20) Kisseleva, N.; Kraut, S.; Jäschke, A.; Schiemann, O. *HFSP J.* **2007**, *1*, 127–136.
(21) Kobitski, A. Y.; Nierth, A.; Helm, M.; Jaschke, A.; Nienhaus, G. U. *Nucleic Acids Res.* **2007**, *35*, 2047.
(22) Varani, G.; Aboul-ela, F.; Allain, F. H. T. *Prog. Nucl. Magn. Reson. Spectrosc.* **1996**, *29*, 51–127.
(23) Wijmenga, S. S.; van Buuren, B. N. M. *Prog. Nucl. Magn. Reson. Spectrosc.* **1998**, *32*, 287–387.
(24) Fürtig, B.; Richter, C.; Wöhnert, J.; Schwalbe, H. *ChemBioChem* **2003**, *4*, 936–62.
(25) Kühn, T.; Schwalbe, H. *J. Am. Chem. Soc.* **2000**, *122*, 6169–6174.
(26) Wirmer, J.; Kühn, T.; Schwalbe, H. Angew. Chem., Int. Ed. 2001.
(27) Zeeb, M.; Balbach, J. *Methods* **2004**, *34*, 65–74.
(28) Fürtig, B.; Buck, J.; Manoharan, V.; Bermel, W.; Jaschke, A.; Wenter, P.; Pitsch, S.; Schwalbe, H. *Biopolymers* **2007**, *86*, 360–83.
(29) Wenter, P.; Bodenhausen, G.; Dittmer, J.; Pitsch, S. *J. Am. Chem. Soc.* **2006**, *128*, 7579–7587.
(30) Höbartner, C.; Micura, R. *J. Mol. Biol.* **2003**, *325*, 421–31.
(31) Höbartner, C.; Mittendorfer, H.; Breuker, K.; Micura, R. *Angew. Chem., Int. Ed.* **2004**, *43*, 3922–5.
(32) Wenter, P.; Fürtig, B.; Hainard, A.; Schwalbe, H.; Pitsch, S. *Angew. Chem., Int. Ed.* **2005**, *44*, 2600–2603.
(33) Wenter, P.; Fürtig, B.; Hainard, A.; Schwalbe, H.; Pitsch, S. *ChemBioChem* **2006**, *7*, 417–420.
(34) Buck, J.; Fürtig, B.; Noeske, J.; Wöhnert, J.; Schwalbe, H. *Proc. Natl. Acad. Sci. U.S.A.* **2007**, *104*, 15699.
(35) Mayer, G.; Heckel, A. 2006, *45*, 4900−4921.
(36) Mok, K. H.; Nagashima, T.; Day, I. J.; Jones, J. A.; Jones, C. J. V.; Dobson, C. M.; Hore, P. J. *J. Am. Chem. Soc.* **2003**, *125*, 12484–12492.

HPLC.[38] The obtained RNA was freeze-dried and desalted using centricon-10 microconcentrators (Amicon). Folding of the RNA was achieved by denaturing at 95 °C followed by 10-fold dilution, cooling on ice cold water for an hour and verified by native gel electrophoresis (see Supporting Information, Figure S1). Finally, the folded RNA was exchanged into the NMR buffer containing 25 mM Tris-HCl buffer at pH 7.5 using Centricon-10 microconcentrators. The chemically synthesized unlabeled A27 WT was purchased from Chemical Synthesis Service (Craigavon, UK).

NMR Data Acquisition for Static NMR Experiments. NMR measurements were performed on Bruker 600, 700, 800, and 900 MHz spectrometers with 5 mm HCN cryogenic probes and *z*-axis gradients. Bruker Topspin and Accelyrs Felix2004 software programs were used for data processing and analysis. All NMR samples contained 10% D_2O and were measured at a temperature of 288 K, except when otherwise stated. The final RNA concentrations ranged between 0.2 and 0.9 mM as determined by UV spectroscopy at 260 nm. For the bound state, we used AMDA (anthracene-maleimidocaproic acid Diels−Alder adduct) as a Diels−Alder product.[16] The compound was dissolved in DMSO (dimethyl sulfoxide) for better solubility prior to complex formation. Therefore, all RNA samples contained DMSO at a concentration of ∼1%. The ^{1}H,^{1}H NOESY[39] spectra of the A27 WT was measured with a mixing time of 80 ms at a temperature of 283 K, while a mixing time of 150 ms was used for ^{1}H,^{1}H NOESY spectra of the G27 MUT. ^{1}H,^{15}N HSQC[23,24] and HNN-COSY[40] experiments measured for G27 MUT were performed as given in refs 40 and 41. The software packages XWINNMR, Topspin and Sparky[42] were used for processing and analyzing experimental data.

Rapid Sample-Mixing Induced Time-Resolved NMR. The rapid sample-mixing time-resolved NMR experiments were setup as described in ref 36. A 50 μL volume of 50 mM Ca^{2+} in NMR buffer (pH 7.5) was injected into 330 μL of NMR buffer containing 0.43 mM RNA and 1 mM AMDA in 10% D_2O. The final concentrations were between 0.37 mM for RNA, 0.7 mM for AMDA, and 8 mM for Ca^{2+}. The NMR experiments consisted of a pseudo-3D experiment of two planes with 128 1D spectra each. A single injection of 50 ms duration followed the recording of the first plane and the second plane thus monitored Ca^{2+} induced folding with a time resolution of 2.2 s. The pseudo-3D data set was Fourier-transformed with 4000 data points in the direct dimension after multiplication with a squared cosines window function. The resulting 1D spectra were submitted to phasing, polynomial baseline correction and peak-integration of the imino-proton signals in the chemical shift range 9−15 ppm. For the kinetic analysis, the baseline corrected and normalized peak intensities were plotted as a function of time. The residual baseline was determined by averaging the intensity values of the first 256 premix scans, (recorded before injection) at the position of the selected signal and subtracting this from the scans recorded after mixing. In addition, corrections for baseline distortions caused by fluid turbulence after injection were performed. The baseline was determined by averaging the area under the curve in a position where no peaks were observed and subtracting this area from both rising and decaying peaks. Normalized imino proton signal intensities were plotted as a function of time. All rates obtained were from biexponential fits of the data using SigmaPlot 10. FELIX (Accelrys) software was used for processing and analyzing the kinetic data.

Results

Ligand-Free A27 WT Adopts a Single Thermodynamically Stable Secondary Structure. In order to characterize the ribozymes under conditions where tertiary structure formation is negligible,[19] NMR spectra were recorded at pH 7.5 in the absence of divalent ions and the Diels−Alder product as ligand. Eleven canonical GC, two noncanonical GU (G13, G35) and two canonical AU (U6, U30) basepairs were observed in the ^{1}H,^{15}N HSQC experiment of the A27 WT ribozyme (see black peaks in Figure 1). Using these data along with a ^{1}H,^{1}H NOESY spectrum, stems I, II, and III shown in blue, yellow, and green, respectively, in Figure 1 could be assigned. The chemical shift assignment and identification of base-pairing interaction corresponded very well with the most stable secondary structure predicted by mfold[43,44] (see Supporting Information, Figure S2 for the NOESY spectrum and entry 3 in Table S2 of the Supporting Information for NMR experimental parameters).

Ligand-Free G27 MUT Adopts Two Stable Secondary Structures. In contrast, NMR spectra of the G27 MUT ribozyme (red NMR cross peaks in Figure 1) showed several additional peaks with different intensities in the ^{1}H,^{15}N HSQC (Figure 1) and ^{1}H,^{1}H NOESY experiments (Figure 2) suggesting the existence of more than a single conformation. These conformations are in slow conformational exchange on the NMR time scale. The NMR data are in agreement with mfold predictions, since the G27 MUT ribozyme has a predicted minimum energy conformation (Figure 2b, $\Delta G = -25.50$ kcal/mol at 310 K) that is different from the conformation prediction for the wild-type ribozyme (Figure 2c, $\Delta G = -24.60$ kcal/mol at 310 K). From a HNN-COSY experiment that reports on the donor and acceptor nitrogen atoms in basepairs, all basepairs in the ligand-free G27 MUT form could be assigned to be of Watson−Crick type. Figure 2a shows the sequential NOESY walk for the assignment of the secondary structure of the G27 MUT ribozyme as continuous blue and green lines for stems I and II, respectively. A further sequential walk could be carried out, and the correlation peaks observed were consistent with the base-pairing pattern of blue stem I and involved weaker resonances (dotted blue line in Figure 2a). The similarity of the chemical shift pattern to the walk indicated by the solid blue line and the involvement of an AU basepair (established by HSQC) excluded the possibility of this walk belonging to yellow stem II. In the C2H2 region (150 ppm) of the ^{1}H,^{13}C HSQC, the number of crosspeaks should directly correlate with the number of six adenine nucleotides in the ribozyme. However, eight resolved signals were observed instead of the expected six resolved signals for a single conformation, reflecting the conformational heterogeneity of the system. These findings lead to the conclusion that the free-form of the G27 MUT ribozyme exists in a major and a minor conformation. ΔG_{exp} at 283 and 288 K were 0.45 and 0.28 kcal/mol, respectively, and were derived from

(37) Stoldt, M.; Wöhnert, J.; Ohlenschläger, O.; Görlach, M.; Brown, L. R. *EMBO J.* **1999**, *18*, 6508–6521.
(38) Pingoud, A.; Fliess, A.; Pingoud, V. *Anal. Bioanal.Chem.* **1987**, *327*, 22–23.
(39) Stonehouse, J.; Shaw, G. L.; Keeler, J. *J. Biomol. NMR* **1994**, *4*, 799–805.
(40) Dingley, A. J.; Grzesiek, S. *J. Am. Chem. Soc.* **1998**, *120*, 8293–8297.
(41) Noeske, J. R., C.; Grundl, M. A.; Nasiri, H. R.; Schwalbe, H.; Wöhnert, J. *Proc. Natl. Acad. Sci. U.S.A.* **2005**, *102*, 1372–1377.
(42) Goddard, T. D.; Kneller, D. G. *SPARKY*; University of California, San Francisco.
(43) Zuker, M. *Nucleic Acids Res.* **2003**, *31*, 3406–3415.
(44) Mathews, D. H.; Sabina, J.; Zuker, M.; Turner, D. H. *J. Mol. Biol.* **1999**, *288*, 911–940.

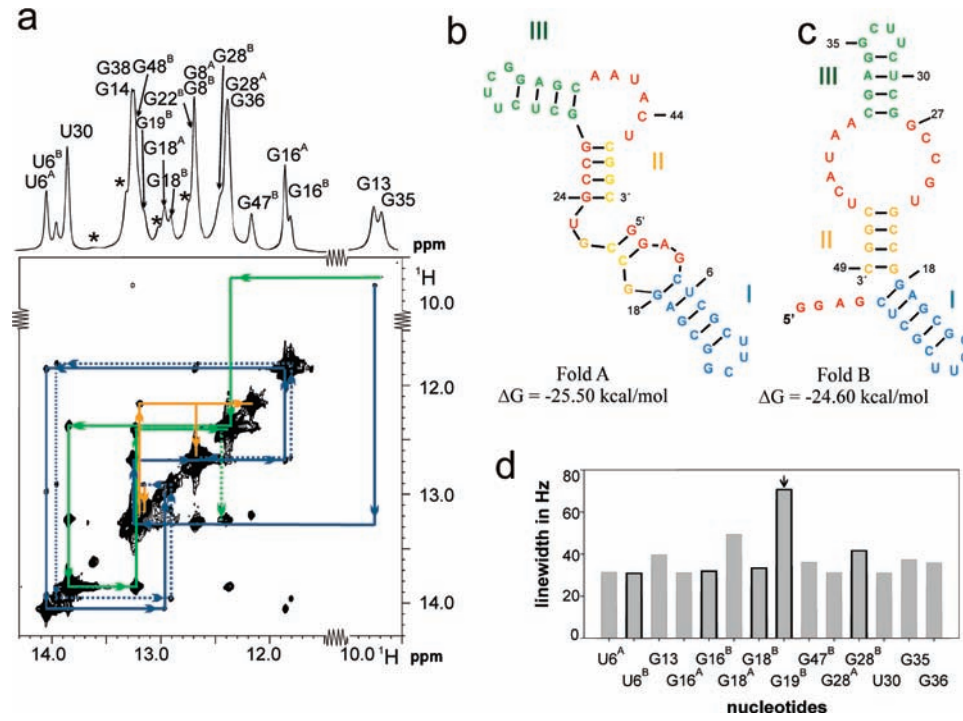

Figure 2. (a) NOESY spectrum of the G27 MUT ribozyme in the absence of ligand and divalent ions (for experimental parameters see entry 4 in Table S2 in the Supporting Information.) Each segment of the sequential walk is color-coded according to the color code of the free state layout that is given in b and c. The dotted blue line denotes the sequential walk assigned to fold B (c). The projection at the top gives the labels of all identified imino resonances. The asterisk labels all unassigned peaks in the imino region. Superscripts A and B identify fold A and fold B peaks. (b, c) The two lowest energy folds of the mutant ribozyme predicted by mfold.[43,44] (d) Bar chart showing the line widths extracted from $^{1}H,^{15}N$ HSQC spectra of the imino protons of the free G27 MUT ribozyme at 283 K. Bars with dark borders denote fold B (c) line widths. The arrow labels $G19^{B}$ line width.

the intensities of the well-resolved resonances from the two folds. The experimental data compare reasonably well with the predictions from mfold.

The yellow stem II of fold B was assigned and showed stacking interactions with the blue stem I similar to the free form of the wild-type ribozyme. As fold B of G27 MUT had exactly the same resonance pattern as that found in the A27 WT including the stacking interaction between stems I and II, we conclude that it has the same conformation as the free-form conformation of A27 WT ribozyme, which is in agreement with the predicted mfold secondary structure (see Figure 2c).

Free Form Conformation of G27 MUT Shows Increased Dynamics in Stem II. The imino proton resonance spectra may also provide information about the dynamics of the RNA. The line width of the imino resonances increases as the hydrogen bonding strength of the respective base pair weakens. Figure 2d shows the ^{1}H line width distribution of imino resonances of the free form G27 MUT extracted from $^{1}H,^{15}N$ HSQC spectrum. The bars with thick black lines correspond to resonances from fold B. The line width of the imino $G19^{B}$ proton of the G27 MUT minor conformation (marked by an arrow in Figure 2d) is almost twice the average value. We conclude that G19 in fold B is involved in weak hydrogen bonding interactions. As A27 WT did not show major line widths variations (20 ± 3 Hz), the increased line width of the $G19^{B}$ imino proton in the G27 MUT is likely not due to "fraying" of terminal base pairs but hints at additional line broadening induced by conformational exchange that is on a slower time scale than fraying motions.

Divalent Metal Binding Induces Tertiary Folding in the Absence of Ligand. The Diels−Alder ribozyme is active only in the presence of divalent ions. We therefore performed a Ca^{2+} titration to characterize the changes in the free form induced by divalent ions for the A27 WT and G27 MUT ribozymes. In the absence of the ligand AMDA, three conformations were identified for G27 MUT. The increased line broadening for resonances of folds A and B reveals increased dynamics of the two folds and a change in their relative population. In addition, the appearance of a signal $U6^{C\text{-like}}$ could be detected at a similar resonance position as in the complex. However, no non-Watson−Crick basepairs that characterize the complex ribozyme for both A27 WT and G27 MUT were detected (Figure 3). The RNA adopts the complex conformation only in the presence of both divalent ions and the Diels−Alder product as discussed in the following section.

The induction of conformational dynamics is also observed for the wild-type ribozyme A27 WT as evident from line broadening effects. This broadening may also be due to exchange with a minor secondary fold that is observed at higher temperatures (see Supporting Information, Figure S8).

Tertiary Complex of G27 MUT in Solution Is in Agreement with Crystal Structure. Our initial time-resolved experiments indicated that folding of the A27 WT ribozyme is too fast for time-resolved NMR studies. Therefore, we focused our attention on the G27 MUT variant.

In the complex form, blue stem I was extended by stacking of two basepairs formed by interaction of A3 and G4 of the 5′-terminal tetranucleotides with U45 and C44 of the conserved bulge region. In the NOESY spectrum, this assignment is shown by the red lines continuing from the blue line that ends at G18 (Figure 4a). In the crystal structure of the RNA−ligand complex, the green stem III was also extended by a noncanonical base pair and two three-base interactions formed by the zippering up of the bulge region by the 5′ single-stranded end. Of this

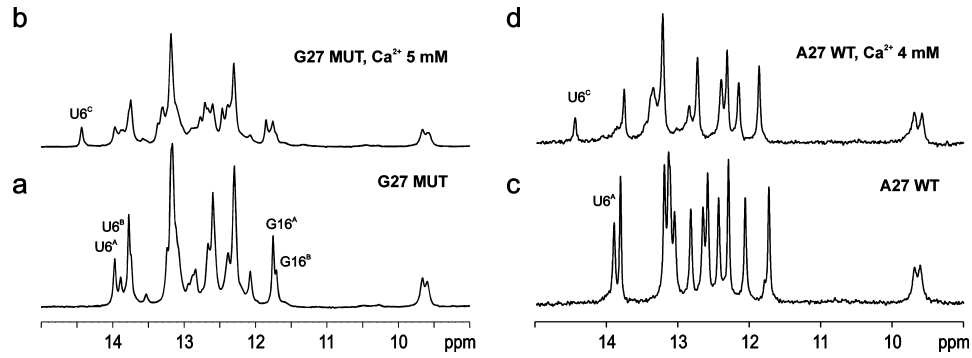

Figure 3. (a, b) Free form and complex form in presence of Ca^{2+} for G27 MUT. (c, d) Free and complex form of A27 WT at 291 K.

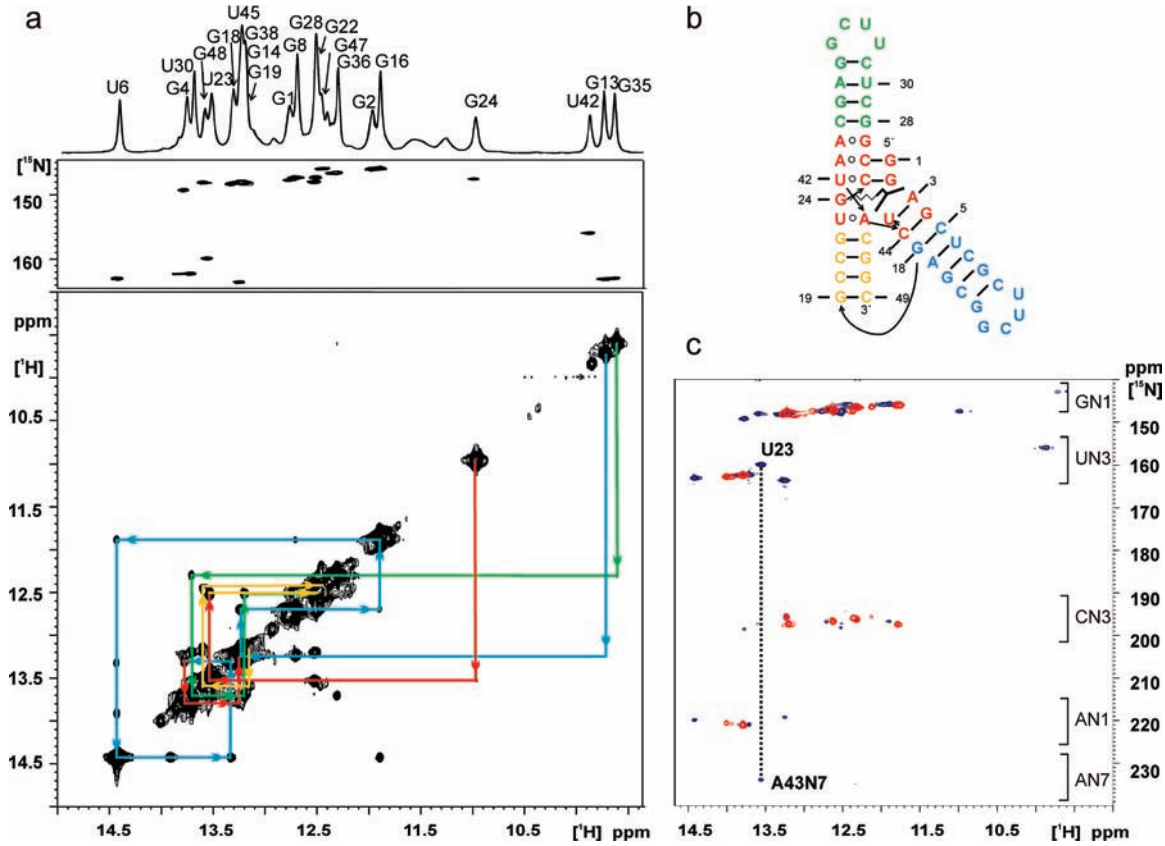

Figure 4. (a) Imino region (15−9 ppm) of the G27 MUT product complex of ^{1}H, ^{1}H NOESY spectrum aligned with ^{1}H, ^{15}N HSQC with the assignment shown (see entries 5 and 6 of Table S2 in the Supporting Information for NMR parameters.) Resonances of G13 and G35 appear folded in the ^{1}H,^{15}N HSQC. (b) Complex structure base-pairing constellation as determined by X-ray crystallography.[19] Color coding is the same as for the free form. (c) Superposition of the HNN-COSY spectra of the free G27 MUT ribozyme in red and the ribozyme in complex with Ca^{2+} and ligand in blue (NMR parameters are given in entries 7 and 8 in Table S2 in the Supporting Information.) The characteristic resonance regions of the base nitrogen atoms of the nucleotides are indicated. The dotted line highlights the reverse Hoogsteen-type basepair between U23 and A43.

extension, only the U42−C25 basepair could be resolved in the NMR spectra. No imino neighbor was detected from G28 to G27 in the NOESY. We attribute this finding to be due to imperfect stacking as observed in the crystal structure. Only a very weak peak was observed at the expected GA base pair resonance region upfield of 11 ppm, the correlation peaks are exchange broadened.

To assign the catalytic core in the complex, we considered the resonance upfield of 11 ppm which could be identified as a G from the ^{1}H,^{15}N HSQC and which could a priori belong to a non-Watson−Crick basepair or even an unpaired G.[22] A crosspeak from this G to a U imino proton, downfield of 13.5 ppm, was observed in the NOESY experiment. This U residue was unambiguously identified as belonging to a reverse Hoogsteen AU base-pair from ^{1}H,^{15}N HSQC and HNN-COSY experiments. The HNN-COSY showed that Watson−Crick side of this U nucleotide was hydrogen bonded with N7 of an A nucleotide (dotted line in Figure 4c). This pattern fits that of G24 and U23-A43 of the conserved region (shown in red) forming a wall of the catalytic pocket. The remaining U resonating in the noncanonical region (from ^{1}H ^{15}N HSQC) at 10 ppm was assigned to U42 that is involved in the base triple with C25 and G2 as observed in the crystal structure. Strong NOESY crosspeaks are observed from the alkyl side chain of the ligand to the imino protons of U23, G24, and A43H_2 and very weak ones to U42. The anthracene rings showed crosspeaks to the imino protons of G2, U45, and A43H_2 (as shown in Supporting Information, Table S1).

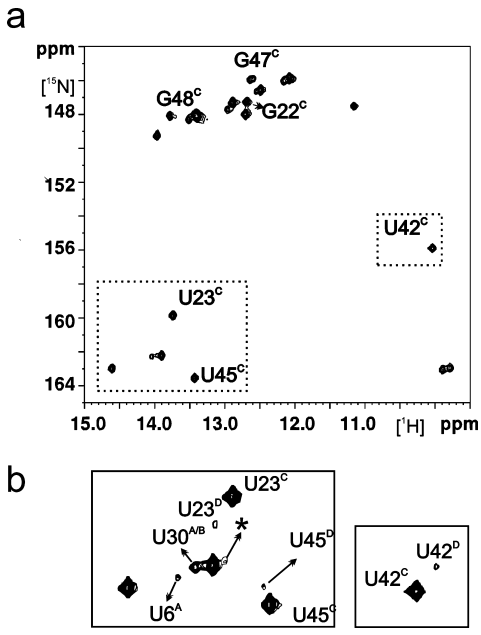

Figure 5. (a) $^{1}H,^{15}N$ HSQC of G27 MUT ribozyme in complex with ligand and Ca^{2+} ions (entry 6 in Table S2 in the Supporting Information gives experimental parameters.) Annotated cross peaks indicate resonances from the major fold C of complex population that also exhibit additional cross peaks originating from fold D of the weaker minor population. (b) Boxed sections of the spectra in b at lower S/N showing weak resonances from fold D, the alternative complex conformation. Also labeled are peaks from residual free ribozyme. $U6^{A}$ is residual peak from fold A of the free form. Peaks arising from the less populated fold D are labeled with a suffix D. The asterisk denotes unassigned peaks.

G27 MUT Complex Displays Conformational Heterogeneity. The $^{1}H,^{15}N$ HSQC of the complex showed a set of additional weak crosspeaks in the noncanonical resonance region belonging to the nucleotides from the catalytic pocket, namely U42, U45, and U23. These are labeled with a superscript D in Figure 5b and indicate a second conformation, fold D, in the complex state. The FRET study also revealed conformational heterogeneity even for the A27 WT ribozyme in the complex form. In addition, resonances from the yellow stem II, namely, G22, G47, and G48 also displayed weaker resonances indicating conformational heterogeneity of stem II.

In the NOESY spectrum in the presence of Ca^{2+} and the Diels−Alder product, exchange crosspeaks caused by magnetization transfer were detected for peaks U6 and G47 between the residual free fold B and complex fold C (circled in black in Figure 6). Exchange crosspeaks were also detected for U23 between folds C and D which will be discussed later. The presence of the free state fold B was detected even at Ca^{2+} concentrations above 4 mM and AMDA concentrations up to 2 mM. This observation is consistent with the FRET analysis, which confirmed presence of a small subset of not fully folded molecules at high divalent ion concentration.

Divalent Metal Ion Binding Sites in the G27 MUT−Ligand Complexes. The line-broadening effect of paramagnetic Mn^{2+} ions was exploited to identify the metal ion binding sites of the ribozyme complex by $^{1}H,^{15}N$ HSQC. According to the crystal structure, at least six Mg^{2+} ions stabilize the RNA structure: While Mg1 and Mg2 are involved in the positioning of stems I and II, Mg4 and Mg6 bind in the grooves of blue stem I, Mg3 in the green stem III, and Mg5 binds near G24, the unpaired nucleotide bordering the catalytic pocket. We performed competition experiments adding paramagnetic Mn^{2+} ions that lead to resonance broadening of imino resonances in the vicinity of the metal binding sites.[24] For the complex in the presence of Ca^{2+}, the strongest effect is seen for the resonances of G2, G24, and U42 that were broadened beyond NMR detection upon addition of 5 μM Mn^{2+} to the ribozyme complex (containing 0.220 mM RNA, 4 mM Ca^{2+} and 0.4 mM ligand. Supporting Information, Table S2, entries 9−11 give NMR experimental parameters). G28 also exhibited severe line broadening which is in line with the presence of an Mg^{2+} binding site in its vicinity. The characterization of metal ion binding on A27 WT studied by EPR concluded that the metal ions bind with different affinities.[20] This finding is consistent with our data for G27 MUT, where line width broadening effects were not uniform at all binding sites.

Figure 7a and b illustrates the effects of Mn^{2+} addition on the line widths of resonances of the G27 MUT−ligand complex folded in the presence of Ca^{2+} and Mg^{2+} ions, respectively (see Supporting Information, Table S2, entries 12−14 for experimental details and an overlay of $^{1}H,^{15}N$ HSQC spectra of the RNA in presence of Mg^{2+} and Ca^{2+}). Resonances arising from U23 and G24 were lost in the Mg^{2+} complex and chemical shift differences between the two complexes were also observed for peaks arising from G8, G22, U42, and G47 (see Figure S6a in the Supporting Information). Nevertheless, the $^{1}H,^{13}C$ HSQC of the aromatic region showed that the same conformation is maintained for both complexes including the reverse Hoogsteen base pair (see Supporting Information, Figure S6b). Consequently, the presence of resonance differences in the $^{1}H,^{15}N$ HSQC of the two complex forms points to differences in solvent exchange and conformational exchange differences. This observation may provide clues to the difference in catalytic activity between the two complexes. The activity reduces by 65% when Ca^{2+} is substituted for Mg^{2+}.[12] As has been established previously, metal ions do not directly participate in the reaction.[12] Therefore, the significant difference in activity points to the structural characteristics of the ribozyme, specifically to the dynamics of the catalytic pocket region as an important player in the catalytic efficiency. Catalytic pocket dynamics was also proposed in the FRET study to explain the catalytic properties.[21] The poor spectral resolution of the Mg^{2+} complex indicates a certain degree of structural flexibility which may be essential for rapid binding and release of substrate and product of the reaction.

Characterization of the Kinetics of Ca^{2+}-Induced Folding of G27 MUT by NOESY and Time-Resolved NMR. By NMR, we could detect folding transitions between the free and the complex form of the ribozyme both at equilibrium in NOESY experiments and by time-resolved NMR experiments. For the mutant ribozyme, weak additional signals for the free form could be detected at Ca^{2+} concentrations above 4 mM and AMDA concentrations up to 2 mM. In the NOESY spectrum of the complex in the presence of 4 mM Ca^{2+} and AMDA, exchange peaks caused by magnetization transfer for residues U6 and G47 between the free form B and complex C could be detected. The presence of these exchange peaks directly report the conformational exchange between the fold B of the free form (Figure 2c) and the fold C of the complex form (Figure 3b). The folding of fold B into fold C complex proceeds with a rate constant of $\sim 3\ s^{-1}$ as quantified from the analysis of cross peak to diagonal peak intensities in exchange-induced correlation peaks in the NOESY experiment (mixing time of 150 ms), calculated using eq 29 from the review article of Perrin and Dwyer.[45]

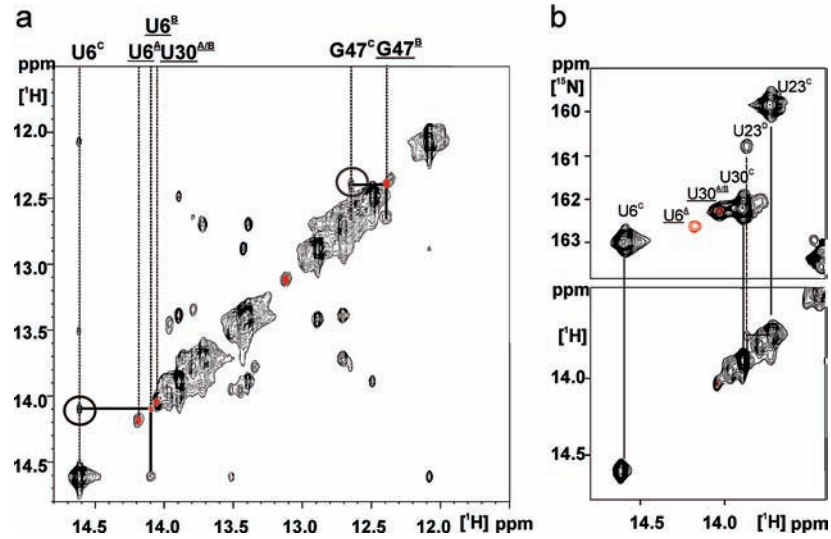

Figure 6. (a) $^{1}H,^{1}H$ NOESY spectrum of imino proton region of G27 MUT complex. Diagonal peaks shown in red arise from residual free form. Exchange crosspeaks above the diagonal between complex and minor free form conformations are circled in black. Residual free form labels are underscored and have a suffix superscript A or B denoting folds A and B, respectively (entry 5 in Table S2 of the Supporting Information gives experiment parameters). (b) Expansion of the imino region of the $^{1}H,^{15}N$ HSQC (on top) and NOESY (bottom) spectra of the region around the U23 chemical shift arising from the G27 MUT ribozyme (0.5 mM) in complex with ligand (2 mM) and Ca^{2+} (4 mM). The vertical lines connect those resonances assigned to the same nucleotides in the two spectra. A weak crosspeak of U23 of fold C in the NOESY is shown by continuous lines. The dotted line connects the resonance labeled $U23^{D}$ in the HSQC arising from a second conformation to the weak exchange crosspeak highlighted in the NOESY. The peaks shown in red arise from residual free form population and their labels underscored.

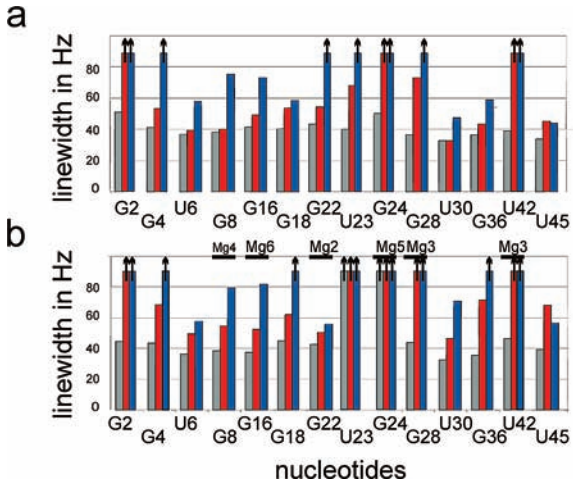

Figure 7. (a) Bar chart giving line widths of imino protons from $^{1}H,^{15}N$ HSQC spectra of the ribozyme−Ca^{2+}−ligand complex in gray. Red and blue bars are line widths obtained on addition of 5 or 10 μM Mn^{2+}, respectively, to the above complex ribozyme. Bars with vertical arrows indicate peak broadening beyond NMR detection. (b) Bar chart giving line widths of imino protons from ^{1}H, ^{15}N HSQC spectra of the ribozyme−Mg^{2+}−ligand complex in gray. Bars with vertical arrows indicate peak broadening beyond NMR detection. Red and blue bars are line widths obtained on addition of 4 and 10 μM Mn^{2+}, respectively, to the above complex ribozyme. Horizontal bars indicate Mg^{2+} binding sites observed in the X-ray structure. The sixth binding site cannot be ascertained due to insufficient chemical shift resolution in the NMR spectra.

We then performed time-resolved NMR experiments to monitor the kinetics of the Ca^{2+}-induced folding to the ribozyme complex. Folding was induced by addition of Ca^{2+} to a sample of RNA already containing ligand[46] (Figure 8c, bottom). This method was preferred over the injection of a mixture of Ca^{2+} and ligand into RNA to prevent ligand precipitation due to insolubility. Efficient mixing was achieved using a pneumatic syringe placed outside the NMR magnet which injects the Ca^{2+} into the NMR tube containing the sample, via a PTFE transfer line.

For the A27 WT ribozyme, folding was fast and was completed in the dead time of the experiment (1.5 s) (data not shown) in reasonable agreement with the FRET study that showed a 100 ms time scale for transitions between RNA states in the absence of ligand.[21] On the other hand, the rates obtained for the G27 MUT were on the order of seconds. Along with slower folding kinetics of the ribozyme mutant, we detected significant conformational heterogeneity both in the free and complex forms of the ribozyme as revealed by the static NMR experiments. We observe at least four conformations, two for the complex (folds C and D in Figure 9a) and two for the free forms (folds A and B in Figure 9). In the presence of Ca^{2+} ions, but without ADMA, the conformational heterogeneity is even more pronounced (Figure 3a and b). Under equilibrium conditions, at least three conformations are observed—a complex-like conformation ($C^{like}\cdot Ca^{2+}$) and two conformations ($A^{like}\cdot Ca^{2+}$ and $B^{like}\cdot Ca^{2+}$) that resemble the free state. The line width of the two conformations $A\cdot Ca^{2+}$ and $B\cdot Ca^{2+}$ is exchange broadened over the entire concentration range of [RNA]/[Ca^{2+}] (see Supporting Information, Figure S7) and thus, the relative ratio [$A\cdot Ca^{2+}$]/[$B\cdot Ca^{2+}$] cannot be determined due to line broadening. In the absence of Ca^{2+}, A27 WT revealed only one free form conformation, while in the presence of Ca^{2+}, additional conformational dynamics are induced (Figure 3c and d).

During the folding of the A27 WT complex, new base pairs are formed including two canonical, two noncanonical, and two base triples. These triples involve long-distance interactions between the unpaired nucleotides of the bulge region and the 5′ tetranucleotide strand, leading to a complex pseudoknot and a cavity that enables substrate binding. The forging of basepairs

(45) Perrin, C. L.; Dwyer, T. J. *Chem. Rev.* **1990**, *90*, 935–967.
(46) NMR spectra showed no changes on addition of ligand to RNA in absence of divalent cations indicating absence of binding. Therefore, in the experiment the pre-mix sample contained RNA and ligand in the ratio ~1:1.5.

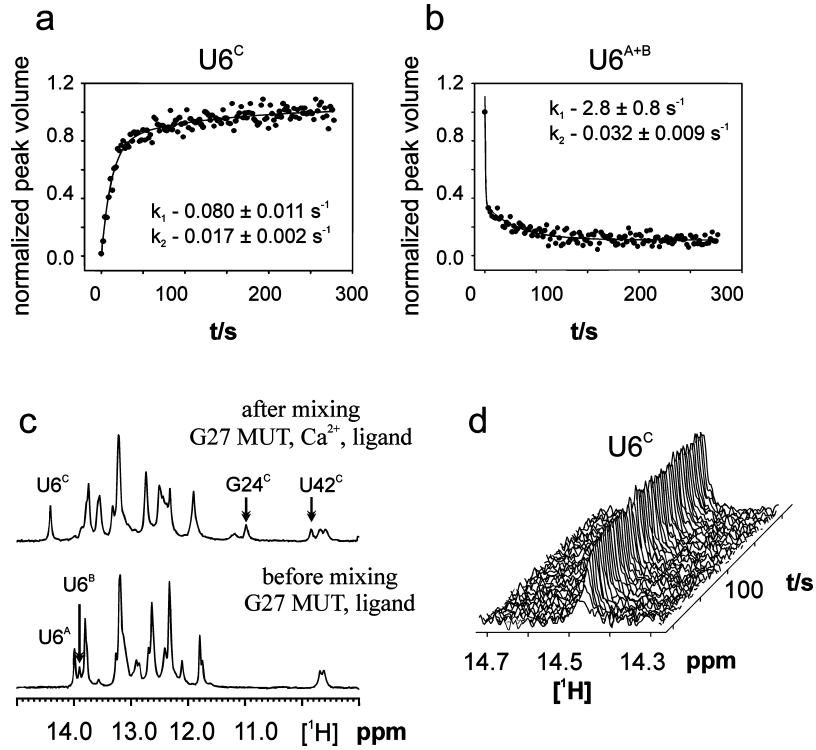

Figure 8. (a) Normalized integrals of resonances of $U6^C$ measured after initialization of folding plotted as a function of time using a double exponential fit. (b) Double exponential fit of $U6^A$ and $U6^B$ resonances arising from the free state of the ribozyme. (c) Top, Imino proton region of 1D of G27 MUT in the presence of ligand in the ratio 1:1.5 before addition of Ca^{2+}. Bottom, G27 MUT in the presence of ligand after injection of Ca^{2+}. (d) Stack plot of imino proton spectra as a function of time of resonance from $U6^C$.

is accompanied by an overall structural rearrangement that involves splaying of the backbone between nucleotides G18 and G19 of stems I and II, respectively.

For the G27 MUT ribozyme, a number of different states are populated after addition of Ca^{2+} to induce folding. For the major free fold A to fold into the complex, six GC basepairs have to be broken before the correct nucleotide pairing of the yellow stem II can be achieved as required for fold C. Therefore, in addition to the long distance interactions as stated above for the A27 WT, four additional GC basepairs have to be formed. Consequently, the rate of formation of the bound complex form should depend strongly on the rate of unfolding of fold A. The characterization of the minor fold B of the free from of G27 MUT revealed an identical fold to the wild-type ribozyme. The unfolding rate of the minor fold of G27 MUT is therefore likely to be similar to the unfolding rate of A27 WT. This hypothesis is supported by the NOESY exchange peaks observed at equilibrium between the minor free fold B and the major complex fold C with a rate constant of $\sim 3\ s^{-1}$.

For the fitting of the rates of folding and unfolding of the G27 MUT detected in the time-resolved NMR experiments, biexponential folding kinetics had to be assumed based on F-statistics analysis. For example, the folding rates toward the complex detected for NMR signal of $U6^C$ arise from a fast ($0.08 \pm 0.011\ s^{-1}$ for 73% population) and a slow transition ($0.017 \pm 0.002\ s^{-1}$ for 27% population). The unfolding rates of $U6^{A+B}$ also revealed second order reactions in the order of 2.8 ± 0.8 (75%) and $0.032 \pm 0.009\ s^{-1}$ (25%) (see Supporting Information, Table S3 for all kinetic rates). It should be noted that the fast rate of unfolding is within the dead time of the experiment.

Discussion and Conclusions

The results of the static and time-resolved NMR experiments conducted in this study were complementary to each other. The results of the time-resolved experiments revealed distinct differences for folding into native state of the ribozymes A27 WT and G27 MUT. Specifically, the folding rates observed for the G27 MUT ribozyme differed by 3 orders of magnitude from the A27 WT folding rates. The differences in the folding rates could be explained with the help of static NMR experiments. The mutant Diels−Alder ribozyme that differs from the most active ribozyme by a single nucleotide reveals an additional energetically favorable conformation fold A in the free state that is slightly more stable than the folding-competent fold B resembling the wild-type free fold. After addition of Ca^{2+}, not only a single conformation is observed, but a heterogeneous ensemble of conformations is adopted of at least three different states: namely $A^{like}\cdot Ca^{2+}$, $B^{like}\cdot Ca^{2+}$, and $C^{like}\cdot Ca^{2+}$. The NMR signals of this counterion-induced ensemble of conformations exhibit increased line widths due to the dynamic interconversion of those states, whose relative populations cannot be determined. From the time-resolved NMR experiments, we can infer that the barriers of interconversion between the states are still high, and therefore, we deduce structural information of the folds $A^{like}\cdot Ca^{2+}$ and $B^{like}\cdot Ca^{2+}$ from the characterization in the absence of Ca^{2+}. Since fold A is stabilized by a different pattern of base pairs, the energetic barrier for conversion of this second fold into the catalytically active fold is high, likely because several base pairs need to be broken and formed; this leads to

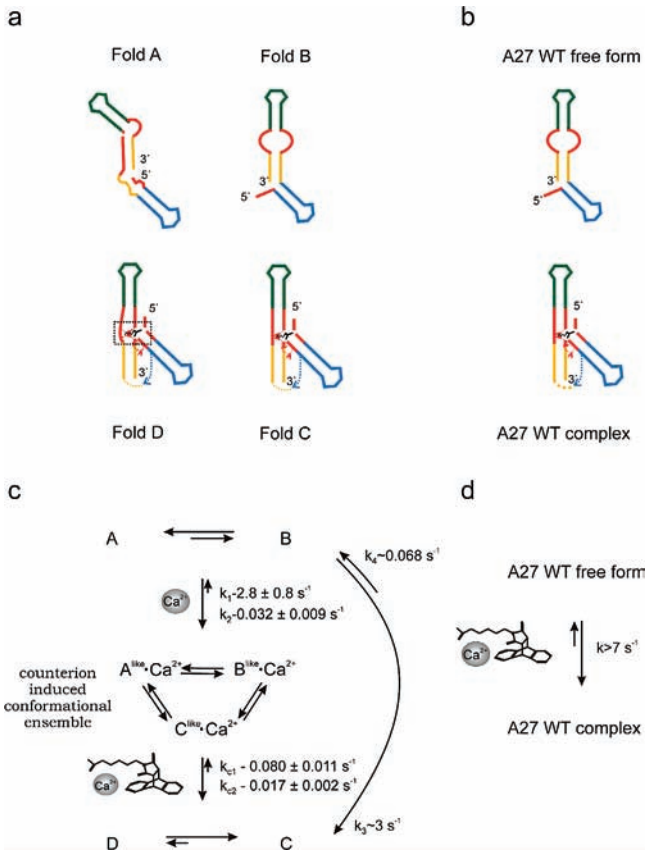

Figure 9. (a) Cartoon representation of the folds as determined from static NMR experiments. A and B are the free form of the ribozyme and C and D the complex form, D being a minor conformation in the complex form with conformational differences centered around the catalytic core. Fold D is in slow exchange with fold C. (b) Cartoon representation of the folds of A27 WT in free form and complex form. (c) Folding model derived on the basis of NMR experiments for G27 MUT ribozyme. The relative concentration of A and B are 3:1. On addition of cations and ligand, conformations A and B assume a counterion-induced ensemble of conformations, A^{like}·Ca^{2+}, B^{like}·Ca^{2+}, and C^{like}·Ca^{2+} which in turn fold into catalytically active fold C. k_1 and k_2 are rates of unfolding of $U6^{A+B}$, k_{c1} and k_{c2} are rates of folding of $U6^{C}$. k_3 and k_4 are derived from the sum of forward and reverse rates which is obtained from the analysis of exchange induced NOE crosspeaks and K_{eq} obtained from the relation K_{eq} = Fold C/Fold B. (d) Folding model of the A27 WT consistent with NMR data presented here and previously published FRET analysis.

a decrease of the overall folding rate in the G27 MUT system. The fundamental rate-limiting step here points to the rearrangement of secondary structures in a compact state rather than a folding mechanism involving tertiary structural rearrangements. Such behavior is not unprecedented, as both the isolated P5abc domain with a three-way junction from the *Tetrahymena* ribozyme[47] and the hairpin ribozyme of the satellite RNA of tobacco ringspot virus[48] showed local secondary structure rearrangement during Mg^{2+} induced folding.

In addition, the time-resolved experiments provide additional insight into the folding event. We observed biexponential kinetics without sigmoidal phase for the folding of the complex state, composed of a fast phase and a slow phase in line with the heterogeneous conformations observed for the free ribozyme. The rates for complex formation detected for the NMR signal of $U6^{C}$ are 0.08 ± 0.011 s^{-1} with 73% amplitude and a slow rate of 0.017 ± 0.002 s^{-1} with 27% amplitude. Despite the limited signal-to-noise in our experiments, the kinetic amplitudes of the two phases, however, are not identical to the 3:1 ratio of populations in the free state. If molecules adopting fold A were revealing slow folding kinetics, then the amplitudes of the slow phase should be 75%. To explain this, we considered the following two additional aspects of our data. From the time-resolved experiments, we had additional information on the unfolding rates (2.8 ± 0.8 (75%) and 0.032 ± 0.009 s^{-1} (25%)) of the two folds. The amplitudes are in agreement with the kinetic rates reporting on complex formation. From the rate obtained from the NOESY spectrum, the folding from fold B to the complex fold C proceeds at a time scale of ~3 s^{-1}. Due to similarity of fold B to the fold of the free state of A27 WT, this conclusion is also strengthened by the results of A27 WT from both NMR and FRET studies. The signal-to-noise for NMR resonances reporting on unfolding is higher than for peaks associated with folding. Therefore, we are not able to detect the fast folding phase in the time-resolved experiments but only in the NOESY exchange spectra.

Since there is no evidence of a sigmoidal phase in the kinetics, the data do not provide evidence for a folding intermediate but rather suggest a complex folding mechanism with different rate constants for different conformations, once folding-competent conditions have been established after the addition of divalent cations. Therefore, we interpret the fast rate of 2.8 ± 0.8 s^{-1} to arise from a divalent counterion-induced rapid collapse of both folds A and B of the ribozyme into at least three folds, A^{like}·Ca^{2+}, B^{like}·Ca^{2+}, and C^{like}·Ca^{2+}. Such counterion-induced collapse has been reported for other RNAs[49−51] In fact, rapid counterion-induced collapse in RNA folding is reported to induce an ensemble of heterogeneous compact conformations before the tertiary structure formation is stabilized. In such compact states, RNAs displaying interactions similar to the native final fold show faster folding kinetics while unfavorably folded compact conformations fold slower as is also observed in our system from the folding rates of 0.08 ± 0.011 and 0.017 ± 0.002 s^{-1} for fold C. Therefore we cannot delineate the folding pathways of the two folds A and B into the native tertiary complex fold C given our data resolution and in light of the existence of a collapsed state.

In summary, our work considerably advances the application of time-resolved NMR spectroscopy to study biomolecular folding reactions, since for the first time RNA pseudoknot folding could be investigated by NMR spectroscopy. On the basis of our results, several factors appear to contribute to the 30% reduction of catalytic activity of the G27 MUT in comparison to the wild-type.

(i) In the mutant ribozyme, the interaction between the Diels−Alder product and the RNA is weakened, and the ensemble displays conformational heterogeneity. We were able to identify at least one weakly populated conformation (D in Figure 9a), which is found to be in slow exchange with major complex population, with the difference in folding centering in the catalytic pocket and the yellow stem II regions.

(47) Wu, M.; Tinoco, Jr. I. *Proc. Natl. Acad. Sci. U.S.A.* **1998**, *95*, 11555–11560.
(48) Rupert, P. B.; Ferré-D'Amaré, A. R. *Nature (London)* **2001**, *410*, 780–786.
(49) Russell, R.; Millett, I. S.; Doniach, S.; Herschlag, D. *Nat. Struct. Mol. Biol.* **2000**, *7*, 367–370.
(50) Deras, M. L.; Brenowitz, M.; Ralston, C. Y.; Chance, M. R.; Woodson, S. A. *Biochemistry* **2000**, *39*, 10975–10985.
(51) Russell, R.; Millett, I. S.; Tate, M. W.; Kwok, L. W.; Nakatani, B.; Gruner, S. M.; Mochrie, S. G. J.; Pande, V.; Doniach, S.; Herschlag, D.; Pollack, L. *Proc. Natl. Acad. Sci. U.S.A.* **2002**, *99*, 4266–4271.

(ii) The equilibrium between free and bound state of G27 MUT is shifted compared to wild-type and ~10% population of the free form can still be detected, leading to a decrease in activity.

(iii) The major complex (fold C in Figure 9a) is also in exchange with the minor conformation (fold B) of free form, which can be directly detected in the NOESY spectrum. Taken together with the lack of stacking interactions between the green stem III and the base pairs formed between nucleotides from the asymmetric internal bulge, these findings suggest that the core of the ribozyme is in a dynamic state in solution, a common feature in some ribozymes. For example, this explanation has been proposed in the case of the hammerhead ribozyme[52] on the basis of ^{1}H and ^{31}P NMR,[53] ^{19}F NMR,[54] and residual dipolar coupling measurements.[55] Further, the observed differences between the Ca^{2+}- and Mg^{2+}-bound complexes reveal conformational dynamics in the catalytic pocket as an important factor for efficient catalysis.

The detailed NMR analysis detects a number of differences in the structure and conformational dynamics of the single nucleotide mutant of the most efficient Diels−Alder ribozyme. The effect of this single-point mutation is dramatic, as several conformations in the free and the complex state are populated as the result of a single-point mutation. The energetic difference in free enthalpy is small, but the barrier of interconversion is high and therefore prolongs the lifetime of the two free states and of the two bound states of the ribozyme, respectively. Therefore, the slow refolding kinetics of RNAs,[56] compared to the situation for proteins, amplify a small destabilizing effect in the ground-state energies of the ribozymes.

These differences suggest that during the in vitro SELEX procedure, evolution of RNA sequences that rapidly fold into the catalytically active conformation constitutes an important evolutionary restraint to gain high turnover for the best ribozymes. Even single-point mutations lead to very significant differences in folding rates spanning 3 orders of magnitude; these differences are linked to structural differences in the free form of both ribozymes, where the free form of the slower folding mutant ribozyme populates two detectable conformations with high barriers for conformational transition. It is tempting to suggest that optimal fit and fast folding kinetics are evolutionary restraints selected for in the SELEX experiments.

Acknowledgment. We thank Elke Stirnal for laboratory support and J. Gottfried Zimmermann, Christian Richter, and Janina Buck for help with NMR measurements. We also thank Jens Wöhnert, Jonas Noeske, Kai Schlepckow, and Jürgen Graf for valuable discussions. The work was supported by the DFG Sonderforschungsbereich "RNA-Ligand-Interaction", (H.S.), DFG Grant No. JA 794/3 (A.J.), the European Commission (EU-NMR), the Fonds der Chemischen Industrie (H.S. and A.J.), the state of Hesse (BMRZ), and the Studienstiftung des Deutschen Volkes (B.F.).

Supporting Information Available: Gel electrophoresis analysis; NOESY spectra of A27 WT; titration monitored by NMR; catalytic pocket of G27 MUT; ligand and RNA interaction data; ^{1}H, ^{15}N HSQC and ^{1}H, ^{13}C HSQC of RNA complex with Ca^{2+} and Mg^{2+}; complete data set on NMR experimental parameters; and complete kinetic rates from time-resolved NMR experiments. This material is available free of charge via the Internet at http://pubs.acs.org.

JA900244X

(52) Blount, K. F.; Uhlenbeck, O. C. *Annu. Rev. Biophys. Biomol. Struct.* **2005**, *34*, 415–40.
(53) Suzumura, K.; Warashina, M.; Yoshinari, K.; Tanaka, Y.; Kuwabara, T.; Orita, M.; Taira, K. *FEBS Lett.* **2000**, *473*, 106–112.
(54) Hammann, C.; Norman, D. G.; Lilley, D. M. J. *Proc. Natl. Acad. Sci. U.S.A.* **2001**, *98*, 5503-–5508.
(55) Bondensgaard, K.; Mollova, E. T.; Pardi, A. *Biochemistry* **2002**, *41*, 11532–11542.
(56) Fürtig, B.; Wenter, P.; Reymond, L.; Richter, C.; Pitsch, S.; Schwalbe, H. *J. Am. Chem. Soc.* **2007**, *129*, 16222–16229.